# Band structure model and dynamical dielectric function in lowest stages of graphite acceptor compounds

J. Blinowski (*), Nguyen Hy Hau, C. Rigaux, J. P. Vieren

Groupe de Physique des Solides de l'Ecole Normale Supérieure, 24, rue Lhomond, 75231 Paris 05, France

R. Le Toullec

Laboratoire de Physique des Solides, Université Pierre-et-Marie-Curie, Tour 13, 4, place Jussieu, 75230 Paris Cedex 05, France

G. Furdin, A. Hérold, J. Melin

Laboratoire de Chimie Minérale Appliquée, 54027 Nancy Cedex, France

(*Reçu le 25 juillet, accepté le 17 septembre 1979*)

**Résumé.** — Un modèle bidimensionnel de structure de bandes est proposé pour décrire les niveaux électroniques dans les stades 1 et 2 des composés d'accepteur. En utilisant la méthode de la liaison forte, nous incluons les interactions intra et intercouches entre carbones voisins. A partir des énergies et fonctions d'onde des bandes $\pi$ de valence et de conduction, la dépendance en fréquence de la fonction diélectrique complexe est établie. Ce modèle permet de rendre compte quantitativement des récents résultats de la réflectivité optique, dans la région de plasma et à énergie plus élevée, sur différents composés d'accepteurs ($Br_2$, ICl, $SbCl_5$, $AsF_5$). De l'analyse théorique des résultats nous déterminons le coefficient de transfert de charge pour plusieurs variétés de composé.

**Abstract.** — A 2D band structure model is proposed to describe electronic states in the lowest stages ($n = 1, 2$) of GAC. The tight binding method is applied taking into account intra and interlayer nearest neighbour interactions. From the energies and wavefunctions of the $\pi$ valence and conduction bands, the frequency dependence of the complex dielectric function is derived. This model enables us to quantitatively analyse recent results of reflectivity in the region of the plasma edge and at higher energy obtained for various GAC ($Br_2$, ICl, $SbCl_5$, $AsF_5$). From the theoretical fits we deduce the charge transfer coefficient for several classes of GAC.

1. **Introduction.** — The low stages of graphite acceptor compounds (GAC) exhibit metallic reflectance. The observation in the visible and near IR spectrum of well-defined plasma edges depending on stages was previously reported for several GAC, namely $NO_3H$ [1], $SbF_5$ [2] and $AsF_5$ [3] graphite. However, no thorough interpretation of the reflectance data has yet been provided : the first attempt by Fischer *et al.* [1] is based on the simplest Drude model neglecting the frequency dependence of the dielectric function, and assuming the validity of the 3D band structure of pure graphite. However, a specific model has to be elaborated to deal with electronic properties in GAC : as the acceptor distribution in successive intercalated layers (even ordered in two dimensional lattices) is not correlated, these compounds do not possess translational symmetry. This excludes the applicability of standard 3D band structure calculations.

There is strong experimental evidence of the two dimensional character of the carriers in GAC as shown by recent results on quantum oscillations [4] and also by the high anisotropy of the electrical conductivity [5]. We propose a two dimensional band structure model describing electronic states in the lowest stages of GAC : we treat an $n$ stage compound as a collection of independent and equivalent subsystems consisting of n graphite layers limited by two intercalated layers. We assume that the electron transfer from the carbon atoms to the acceptors introduces free delocalized holes in the graphite layers of each subsystem, whereas the negative charge is tightly bound to the acceptors. We exclude the possibility of charge flow across the intercalated layers,

(*) Permanent address : Institute of Theoretical Physics, Warsaw University, 00-581 Warsaw, Hoza 69, Poland.

the distance $I_c$ between the carbon layers adjacent to the intercalated molecules being much larger than the interlayer spacing $d$ between the graphite planes.

We restrict our attention to 1 and 2 stage compounds only. For $n \geqslant 3$, the electrostatic effects related to nonequivalence between graphite layers have to be accounted for. We will consider the case $n \geqslant 3$ in a separate paper.

Electronic states in the lowest stages of GAC are described in section 2. We apply the tight binding method, taking into account interactions between nearest carbon atoms. For the first stage, the band structure corresponds to the 2D model of graphite, with linear in $k$ dispersion relations near the degeneracy point of the $\pi$ bands. In the second stage, the interlayer interaction partially removes the conduction and valence band degeneracy, and consequently several types of interband transitions are predicted in the IR and visible regions.

In section 3, we derive the frequency dependence of the dielectric function for stages 1 and 2 of GAC : real interband transitions whose thresholds are related to the Fermi energy are responsible for a frequency dependent interband contribution, which may drastically influence the reflectivity spectrum. The intraband contribution due to free holes, calculated within our 2D band structure model, exhibits a hole concentration dependence quite different from the case of parabolic bands.

We present, in Sections IV and V, the experimental details and the new results of reflectivity experiments obtained for stage 2 of several GAC ($Br_2$, ICl, $SbCl_5$) in the spectral regions 0.1-3 eV. These results, as well as some of the previous data [3], are quantitatively analysed using the theoretical formulation of the dynamical dielectric function established in section 3. Theoretical fits provide a determination of the hole Fermi energy, and consequently of the charge transfer coefficient, for several varieties of GAC.

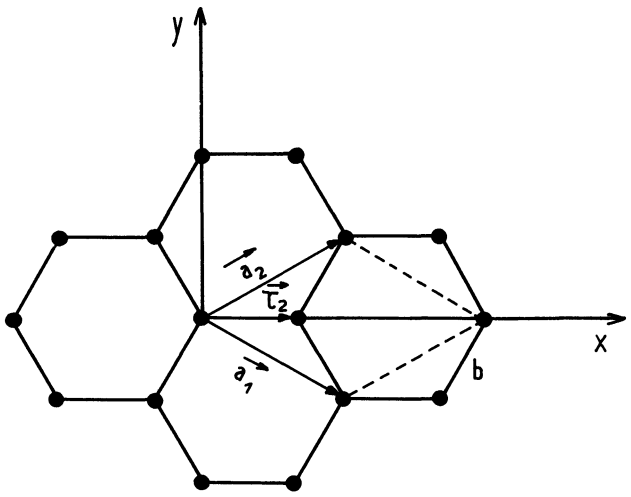


Fig. 1. — Unit cell of a single graphite layer.

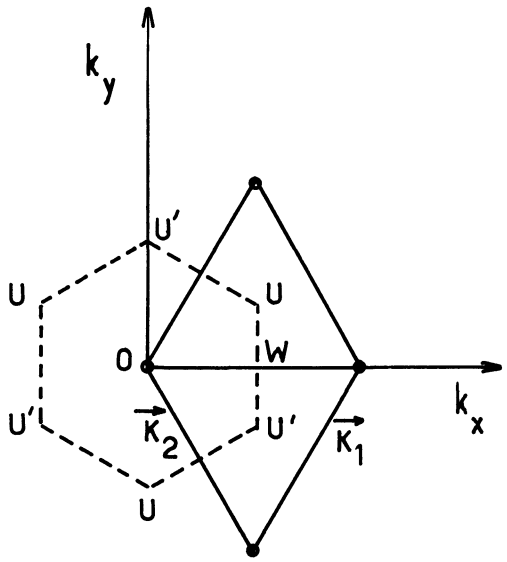


Fig. 2. — Two alternative forms of the Brillouin zone.

2. **Electronic states.** — 2.1 FIRST STAGE. — Within the model of independent graphite sub-systems, the band structure of first stage GAC is directly related to the band structure of 2D graphite, i.e. of a single, neutral graphite layer [6].

In 2D graphite the bands are classified as $\sigma$ (even) or $\pi$ (odd), depending on the symmetry of the wavefunctions with respect to the reflection in the layer plane. The valence electrons of two carbon atoms per unit cell (see Fig. 1) completely fill three $\sigma$ bands and one $\pi$ band.

At the points $U$ and $U'$ of the Brillouin zone (Fig. 2) related by the time reversal operation, the $\pi$ valence band is degenerate by symmetry with the lowest $\pi$ conduction band. Close to the degeneracy points, energy bands are linear, isotropic functions of the wavevector $\mathbf{k} = \boldsymbol{\kappa} - \boldsymbol{\kappa}_U$ (or $\boldsymbol{\kappa} - \boldsymbol{\kappa}_{U'}$). Each band has a saddle point at $W$ and an extremum at 0. All these features, first established by Wallace [6] by a simple tight-binding method, have been later confirmed by far more realistic band structure calculations [7, 8] (see Fig. 3).

The Wallace method consists of the diagonalization of the one-electron Hamiltonian in the subspace spanned by the two simplest tight-binding functions built from atomic 2p orbitals $\varphi_z(\mathbf{r})$ of carbon atoms :

$$U_{i\boldsymbol{\kappa}}(\mathbf{r}) = \sqrt{\frac{\Omega}{\Sigma}} \sum_{\boldsymbol{\rho}_n} e^{i\boldsymbol{\kappa}(\boldsymbol{\rho}_n + \boldsymbol{\tau}_i)} \varphi_z(\mathbf{r} - \boldsymbol{\rho}_n - \boldsymbol{\tau}_i), \quad i = 1, 2 \quad (1)$$

$\Omega$ and $\Sigma$ are the areas of the elementary cell and the crystal, respectively. $\boldsymbol{\kappa}$ is the 2D wavevector, $\boldsymbol{\kappa} = 0$ at the 0 point. $\boldsymbol{\rho}_n = n_1 \mathbf{a}_1 + n_2 \mathbf{a}_2$ is the lattice vector ; $\mathbf{a}_1$ and $\mathbf{a}_2$ the primitive translation vectors. $\boldsymbol{\tau}_1$ and

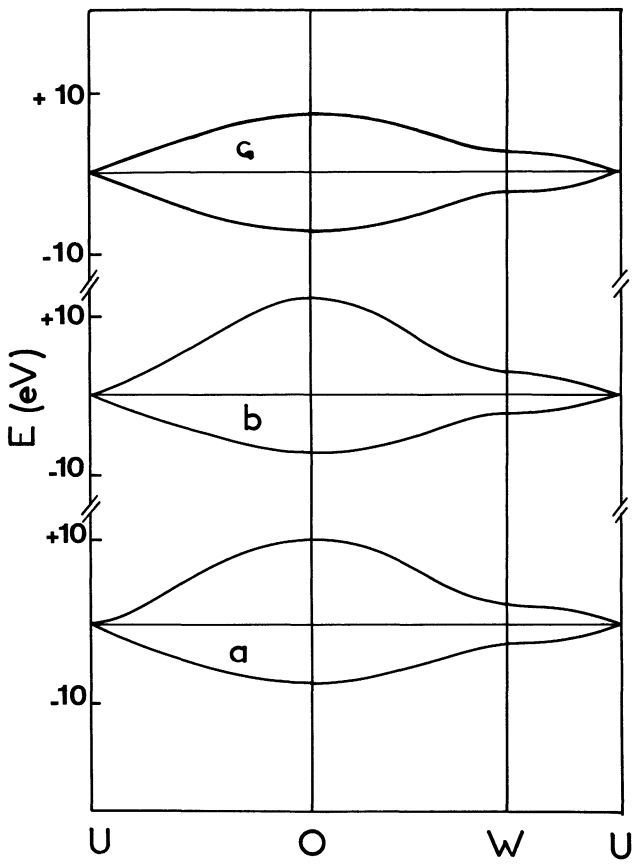


Fig. 3. — Energy band structure of 2D graphite along the principal directions in the Brillouin zone. *a*) Ref. [7]. *b*) Ref. [8]. *c*) Tight binding model of this paper.

$\tau_2$ define the positions of atoms in a unit cell. In the coordinate system adopted in figure 1

$$\mathbf{a}_1 = \frac{3}{2} b\mathbf{e}_x - \frac{\sqrt{3}}{2} b\mathbf{e}_y, \quad \mathbf{a}_2 = \frac{3}{2} b\mathbf{e}_x + \frac{\sqrt{3}}{2} b\mathbf{e}_y,$$

$$\tau_1 = 0, \quad \tau_2 = \frac{1}{3}(\mathbf{a}_1 + \mathbf{a}_2) = b\mathbf{e}_x$$

where $b = 1.42$ Å is the nearest neighbour distance, $\mathbf{e}_x$, $\mathbf{e}_y$ are the unit vectors of coordinate axes.

When the overlaps and resonance integrals for all except nearest neighbours are neglected, the secular equation is :

$$\det \begin{bmatrix} -E & -(\gamma_0 + SE)\, g(\boldsymbol{\kappa}) \\ -(\gamma_0 + SE)\, g^*(\boldsymbol{\kappa}) & -E \end{bmatrix} = 0 . \tag{2}$$

In this equation $S$ is the overlap integral

$$S = \int \varphi_z(\mathbf{r})\, \varphi_z(\mathbf{r} - \tau_2)\, \mathrm{d}^3 r .$$

The resonance integral $\gamma_0$ is defined as :

$$\gamma_0 = -\int \varphi_z(\mathbf{r}) \left[V(\mathbf{r}) - V_{at}(\mathbf{r})\right] \varphi_z(\mathbf{r} - \tau_2)\, \mathrm{d}^3 r + S \int \varphi_z(\mathbf{r}) \left[V(\mathbf{r}) - V_{at}(\mathbf{r})\right] \varphi_z(\mathbf{r})\, \mathrm{d}^3 r$$

where $V(\mathbf{r})$ and $V_{at}(\mathbf{r})$ are the crystal, and the atomic potentials respectively. The energy at the $U$ point is chosen as the origin of the scale. The function $g(\boldsymbol{\kappa})$ is :

$$g(\boldsymbol{\kappa}) = \mathrm{e}^{i\boldsymbol{\kappa}\tau_2} + \mathrm{e}^{i\boldsymbol{\kappa} D_3 \tau_2} + \mathrm{e}^{i\boldsymbol{\kappa} D_3^{-1} \tau_2}$$

where $D_3$ is the operator of the $\frac{2\pi}{3}$ rotation around the $c$ axis. $g(\boldsymbol{\kappa})$ is equal to 3 at the 0 point, 1 at $W$ and $O$ at $U$ and $U'$.

In the region of $\boldsymbol{\kappa}$-space where

$$S \mid g(\boldsymbol{\kappa}) \mid \ll 1 \tag{3}$$

the terms proportional to $S$ in (2) can be neglected and the energies and wavefunctions for both $\pi$ bands are given by simple formulae

$$E_{c,v}(\boldsymbol{\kappa}) = \pm \gamma_0 \mid g(\boldsymbol{\kappa}) \mid \tag{4}$$

$$\psi_{c,v\boldsymbol{\kappa}} = \frac{1}{\sqrt{2}} \left[ U_{1\boldsymbol{\kappa}} \mp \frac{g^*(\boldsymbol{\kappa})}{\mid g(\boldsymbol{\kappa}) \mid} U_{2\boldsymbol{\kappa}} \right]. \tag{5}$$

The upper and lower signs in (4, 5) correspond to the conduction ($c$) and valence ($v$) bands, respectively.

In figure 3*c* we plot the dispersion relations (4) for principal directions in the Brillouin zone. If the value $\gamma_0 = 2.4$ eV is adopted, then the simple formula (4) reproduces fairly well the shape of the bands even far from the $U$ point, where the strong inequality (3) is no longer valid. In the vicinity of $U$, where

$$k = \mid \mathbf{k} \mid = \mid \boldsymbol{\kappa} - \boldsymbol{\kappa}_u \mid \lesssim \frac{1}{3} \mid \boldsymbol{\kappa}_u - \boldsymbol{\kappa}_w \mid \tag{6}$$

the function $g(\boldsymbol{\kappa})$ can be well approximated by

$$g(\boldsymbol{\kappa}) \cong \frac{3}{2} b(k_x - i k_y) \tag{7}$$

and the band energies become linear isotropic functions of $\mathbf{k}$ (Fig. 4) :

$$E_{c,v}(\mathbf{k}) = \pm \frac{3}{2} \gamma_0 bk . \tag{8}$$

In the following, we restrict our considerations to the vicinity of $U$ the point where eqs. (3), (6), (7), (8) can be applied.

We assume that the positive excess charge at the graphite layers resulting from charge transfer to

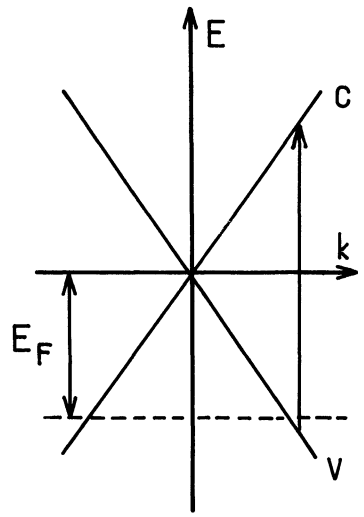


Fig. 4. — Zero gap band structure of the first stage.

acceptors is completely delocalized in the xy plane, but bound in the direction perpendicular to the layer plane. The transfer of one electron creates a free hole in the 2D valence band. For a first stage compound $C_l$ A the number of holes per unit surface may be expressed as :

$$n = \frac{f}{l}\frac{2}{\Omega} \tag{9}$$

where the charge transfer coefficient f is defined as the number of holes per acceptor ; $f/l$ gives the number of holes per carbon atom. We neglect the fluctuations of potential energy induced within each graphite subsystem by the charged acceptors (whose 2D order is generally unknown). These fluctuations should be strongly screened due to the large densities of free holes. In the case of ordered acceptor distributions, even small potential fluctuations impose band folding leading to a reconstruction of the Fermi surface. These effects should however not show up in the visible and near IR spectra.

The positive excess charge at the graphite layers modifies the crystal potential $V(\mathbf{r})$ without changing the symmetry of the system. The band energies and wavefunctions are still given by the formulae (5), (7) and (8) but with the modified value of $\gamma_0$. We estimated the change of $\gamma_0$ due to the excess charge using two methods. In the first method we assumed that the atomic orbitals remain unchanged, we calculated the change in crystal potential due to the partial depopulation of the valence band and therefrom the change of $\gamma_0$. The second method consisted of calculating $\gamma_0$ following the approach proposed by Slonczewski and Weiss [11] but assuming that the effective nuclear charge is increased by the term $f/l$. Both methods are very approximate and lead to corrections of opposite signs, in both cases however the relative changes in $\gamma_0$ are less than about 0.5 $f/l$. It seems therefore that for typical values of $f/l$ in GAC ($f/l < 0.1$) the change of $\gamma_0$ due to the charge transfer is a minor effect and can be neglected. For donor compounds the effect might be more important because of generally higher values of $f$.

For typical values of charge transfer $f/l < 0.1$, the holes in a first stage GAC should occupy (at $T = 0$ K) two separate regions of the 2D Brillouin zone centred at the $U$ and $U'$ points. For $f/l \lesssim 0.05$, the Fermi contours are practically circular. The radii $k_F$ of the Fermi circles and the Fermi energy $E_F$ are given by :

$$k_F = \sqrt{\pi n} = \sqrt{\frac{2\pi}{\Omega}\frac{f}{l}} \tag{10}$$

$$E_F = \frac{3}{2}\gamma_0 b k_F = \gamma_0 \sqrt{\frac{\pi f \sqrt{3}}{l}}. \tag{11}$$

2.2 SECOND STAGE. — In second stage compounds, the arrangement of carbon atoms between successive intercalated layers is the same as in pure graphite (Fig. 5).

In a close analogy with the procedure applied by Wallace [6] for the 3D graphite, we diagonalize the two layer Hamiltonian in the subspace spanned by the functions :

$$U_{i\kappa}(\mathbf{r}) = \sqrt{\frac{\Omega}{\Sigma}} \sum_{\rho_n} e^{i\kappa\cdot(\rho_n+\tau_i)} \times \times \varphi_z(\mathbf{r} - \rho_n - \tau_i), \quad i = 1, 2, 3, 4 \tag{12}$$

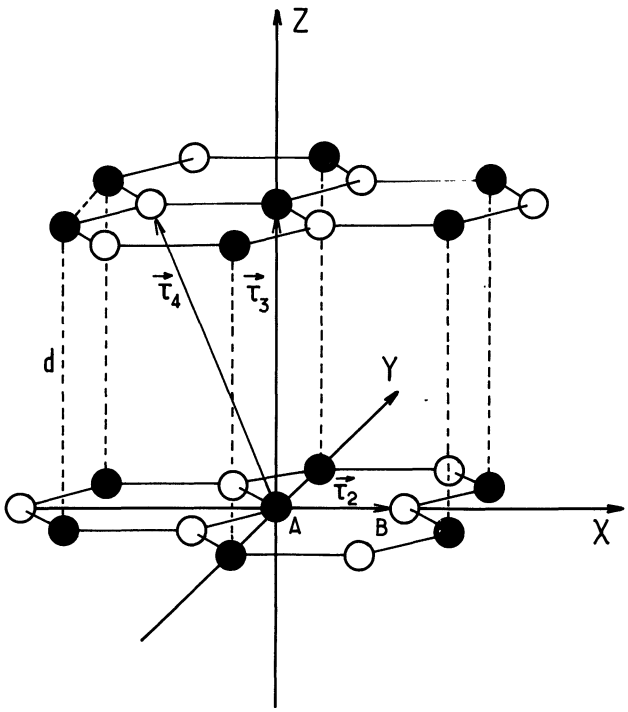


Fig. 5. — Arrangement of carbon atoms in the second stage.

where
$\tau_1 = 0$, $\tau_2 = b\mathbf{e}_x$, $\tau_3 = d\mathbf{e}_z$, $\tau_4 = -b\mathbf{e}_x + d\mathbf{e}_z$
and $d = 3.35$ Å is the interlayer spacing.

In the vicinity of the $U$ point, the corresponding secular equation is :

$$\det \begin{vmatrix} \Delta - E & -\gamma_0 g(\kappa) & \gamma_1 & 0 \\ -\gamma_0 g^*(\kappa) & -E & 0 & 0 \\ \gamma_1 & 0 & \Delta - E & -\gamma_0 g^*(\kappa) \\ 0 & 0 & -\gamma_0 g(\kappa) & -E \end{vmatrix} = 0 \qquad (13)$$

where $\gamma_1$ is the resonance integral for the nearest atoms in two layers ($A - A'$) :

$$\gamma_1 = \int \varphi_z(\mathbf{r}) [V(\mathbf{r}) - V_{at}(\mathbf{r})] \varphi_z(\mathbf{r} - \tau_3) d^3r - S_1 \int \varphi_z(\mathbf{r}) [V(\mathbf{r}) - V_{at}(\mathbf{r})] \varphi_z(\mathbf{r}) d^3r$$

$S_1$ being the $A$-$A'$ overlap integral. $\Delta$ results from the difference of the crystal potential in the vicinity of $A$ and $B$ atoms :

$$\Delta = \int \varphi_z(\mathbf{r}) V(\mathbf{r}) \varphi_z(\mathbf{r}) d^3r - \int \varphi_z(\mathbf{r} - \tau_2) V(\mathbf{r}) \varphi_z(\mathbf{r} - \tau_2) d^3r .$$

In writing down (13) we made several approximations. First, as we restrict our consideration to the vicinity of the $U$ point, we have neglected SE compared to $\gamma_0$ and $S_1 E$ compared to $\gamma_1$. Second we neglected all resonance and overlap integrals for atomic pairs other than intralayer $A$-$B$ and interlayer $A$-$A'$ nearest neighbours. We also disregarded the possible mixing of $\pi$ and $\sigma$ bands.

The valence ($v$) and conduction ($c$) band dispersion relations resulting from (13) are :

$$E_{v_1}(\mathbf{k}) = \frac{1}{2}[\gamma_1 + \Delta - \sqrt{(\gamma_1 + \Delta)^2 + 9\gamma_0^2 b^2 k^2}] ;$$

$$E_{v_2}(\mathbf{k}) = \frac{1}{2}[-\gamma_1 + \Delta - \sqrt{(\gamma_1 - \Delta)^2 + 9\gamma_0^2 b^2 k^2}] ; \qquad (14)$$

$$E_{c_1}(\mathbf{k}) = \frac{1}{2}[-\gamma_1 + \Delta + \sqrt{(\gamma_1 - \Delta)^2 + 9\gamma_0^2 b^2 k^2}] ;$$

$$E_{c_2}(\mathbf{k}) = \frac{1}{2}[\gamma_1 + \Delta + \sqrt{(\gamma_1 + \Delta)^2 + 9\gamma_0^2 b^2 k^2}] .$$

All three band parameters ($\gamma_0$, $\gamma_1$, $\Delta$) depend on the charge transfer coefficient $f/l$ and on the spatial distribution of the excess charge, which in turn depends on the band structure and wavefunctions resulting from (13). In general, the problem has to be solved self-consistently, but according to our estimates the charge transfer typical for GAC does not significantly change the values of $\gamma_0$ and $\gamma_1$. The quantity $\Delta$ is much less important here than in pure graphite, where $\Delta$ is responsible for the *vertical* overlap between valence and conduction bands. In the present case, the effect of $\Delta$ reduces to a small shift of the 2D bands $v_1$ and $c_1$ with respect to $v_2$ and $c_2$ bands. In the following, we simplify (14) putting $\Delta = 0$ (see Fig. 6)

$$-E_{v_1} = E_{c_1} = \frac{1}{2}(\sqrt{\gamma_1^2 + 9\gamma_0^2 b^2 k^2} - \gamma_1) \equiv E_1 .$$

$$-E_{v_2} = E_{c_2} = \frac{1}{2}(\sqrt{\gamma_1^2 + 9\gamma_0^2 b^2 k^2} + \gamma_1) \equiv E_2 \qquad (15)$$

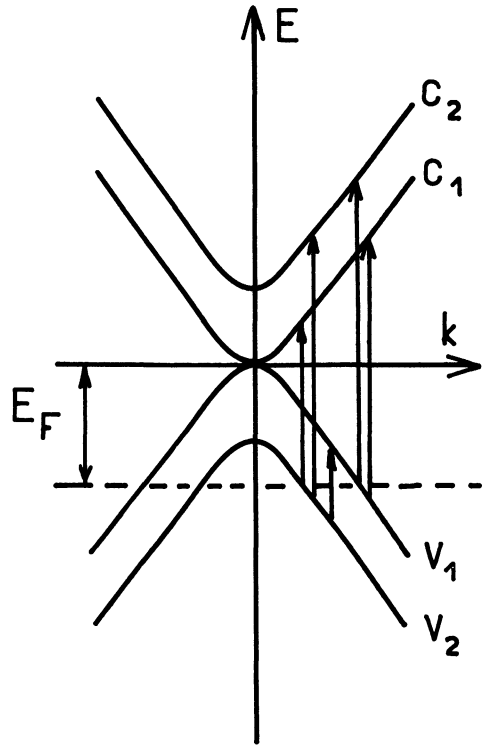


Fig. 6. — Band structure for the second stage.

The corresponding wavefunctions are :

$$\begin{aligned}
\psi_{v_1} &= \frac{1}{\sqrt{2\,E_1(\gamma_1^2 + 9\,\gamma_0^2\,b^2\,k^2)^{1/4}}}[E_1\,U_{1\kappa} + \gamma_0\,g^*\,U_{2\kappa} + E_1\,U_{3\kappa} + \gamma_0\,gU_{4\kappa}] \\
\psi_{c_1} &= \frac{1}{\sqrt{2\,E_1(\gamma_1^2 + 9\,\gamma_0^2\,b^2\,k^2)^{1/4}}}[E_1\,U_{1\kappa} - \gamma_0\,g^*\,U_{2\kappa} - E_1\,U_{3\kappa} + \gamma_0\,gU_{4\kappa}] \\
\psi_{v_2} &= \frac{1}{\sqrt{2\,E_2(\gamma_1^2 + 9\,\gamma_0^2\,b^2\,k^2)^{1/4}}}[E_2\,U_{1\kappa} + \gamma_0\,g^*\,U_{2\kappa} - E_2\,U_{3\kappa} - \gamma_0\,gU_{4\kappa}] \\
\psi_{c_2} &= \frac{1}{\sqrt{2\,E_2(\gamma_1^2 + 9\,\gamma_0^2\,b^2\,k^2)^{1/4}}}[E_2\,U_{1\kappa} - \gamma_0\,g^*\,U_{2\kappa} + E_2\,U_{3\kappa} - \gamma_0\,gU_{4\kappa}]\,.
\end{aligned} \tag{16}$$

Unless the charge transfer coefficient $f/l$ is exceptionally small ($f/l \lesssim 0.01$) both valence bands are populated at $T = 0$ K and the Fermi energy $E_F$ exceeds $\gamma_1$.

The formula relating $E_F$ to $f/l$ reads :

$$E_F = \gamma_0 \sqrt{\frac{\pi f \sqrt{3}}{2\,l}}\,. \tag{17}$$

The ratio of 2D hole densities $n_1$ and $n_2$ in the valence bands $v_1$ and $v_2$ respectively, is given by :

$$\frac{n_2}{n_1} = \frac{k_{F2}^2}{k_{F1}^2} = \frac{E_F - \gamma_1}{E_F + \gamma_1}$$

where $k_{F1}$ and $k_{F2}$ are the Fermi momenta in both bands.

3. **Frequency dependence of the dielectric function.** — To interpret optical properties in GAC, we calculate the frequency dependent dielectric function within the 2D band structure model described in section 2. We treat an n stage compound of dimension $l_z$ in the c direction as $\frac{l_z}{I_c + (n-1)\,d}$ independent and identical two dimensional subsystems parallel to the $xy$ plane. $I_c$ is the distance between the carbon layers adjacent to the intercalants. For light propagating along the c-axis, optical properties of this medium are characterized by the dielectric function $\varepsilon_\perp$ :

$$\varepsilon_\perp = \varepsilon_{\text{inter}} - \sum_j \frac{\omega_j^2}{\omega^2} \tag{18}$$

$-\omega_j^2/\omega^2$ represents the intraband contribution of holes occuping the states in the $j$th band and $\varepsilon_{\text{inter}}$ is the interband contribution.

The general expression for the plasma frequency $\omega_j$ is

$$\omega_j^2 = 4\,\pi e^2\,N_j \frac{1}{\hbar^2}\left\langle \frac{\partial^2 E_j(\mathbf{k})}{\partial k_x^2} \right\rangle \tag{19}$$

where $N_j$ is the 3D hole density which is related to the 2D hole density $n_j$ by :

$$N_j = \frac{n_j}{I_c + (n-1)\,d}\,.$$

The bracket in (19) represents the average over all occupied states in the $j$th band.

For degenerate carriers ($kT \ll E_F$), this bracket can be approximated by

$$\frac{1}{n_j}\frac{4}{4\,\pi^2}\int_{k<k_{F_j}} \frac{\partial^2 E}{\partial k_x^2}\,d^2k$$

where the factor 4 accounts for spin degeneracy and for the existence of two valleys.

The intraband contributions are :

For the first stage,

$$-\frac{\omega_1^2}{\omega^2} = -\frac{4\,e^2\,E_F}{I_c\,\hbar^2\,\omega^2}\,. \tag{20}$$

For the second stage, if $E_F > \gamma_1$

$$-\frac{\omega_1^2}{\omega^2} - \frac{\omega_2^2}{\omega^2} = -\frac{8\,e^2\,E_F}{(I_c + d)\,\hbar^2\,\omega^2}\,\frac{E_F^2 - \frac{\gamma_1^2}{2}}{E_F - \frac{\gamma_1^2}{4}}\,. \tag{21}$$

The expressions (20) (21) exhibit an unusual concentration dependence of the intraband terms : contrary to the case of parabolic bands where $\omega_j^2 \propto N_j$, the intraband contribution is proportional to $E_F$ and therefore to $N_j^{1/2}$.

From the model described in section 2, one may expect important contributions to the dielectric function originating from the interband transitions which start at the energies $\hbar\omega = 2\,E_F$ for the first stage (Fig. 4) and at $\hbar\omega = 2\,E_F$, $2\,E_F \pm \gamma_1$ for the second stage (Fig. 6). Another consequence of the model is an absorption peak corresponding to inter-

valence transitions $v_2 \rightarrow v_1$ expected at $\hbar\omega = \gamma_1$ in 2nd stage compounds. Beyond the absorption thresholds, the imaginary part of the dielectric function cannot be neglected. Its contribution may also affect (via the Kramers-Kronig relation) the frequency dependence of the real part of $\varepsilon_\perp$.

The interband contribution to the complex dielectric function is :

$$\varepsilon_{\text{inter}} - 1 = -\frac{4\pi e^2}{m^2\,\omega(I_c + (n-1)\,d)} \lim_{s\to 0^+} \sum_{j,j'} \frac{2}{(2\pi)^2} \int_{BZ} f(E_j(\mathbf{k}))\,[1 - f(E_{j'}(\mathbf{k}))] \times \times \frac{|P_{j\to j'}|^2}{\omega_{jj'k}} \left[\frac{1}{\hbar\omega_{jj'k} - \hbar\omega - is} - \frac{1}{\hbar\omega_{jj'k} + \hbar\omega + is}\right] \quad (22)$$

where

$$\hbar\omega_{jj'k} = E_j(\mathbf{k}) - E_{j'}(\mathbf{k}) \qquad \text{and} \qquad |P_{j\to j'}|^2 = \frac{1}{2}[|\langle j'k\,|\,P_x\,|\,jk\rangle|^2 + |\langle j'k\,|\,P_y\,|\,jk\rangle|^2]\,.$$

We consider successively the case of the pure graphite, first and second stage compound.

3.1 PURE GRAPHITE. — The dielectric function of pure graphite has been calculated by Johnson and Dresselhaus [9]. Taking into account the overall complexity of the 3D band structure these authors obtained a very good agreement with experimental data. It has been shown however by numerical calculations [10] that the 2D model also gives a correct description of the visible and near IR properties of graphite, neither the density of states nor the transition probabilities being significantly affected by the weak interlayer interaction.

An approximate analytical formula for $\varepsilon_{\text{inter}}$ in the 2D model can be obtained using (22) with $n = 1$ and $I_c = d$. From the wavefunctions (5) and from the $\mathbf{k}.\pi$ expression for $\gamma_0$ derived by Slonczewski and Weiss [11], the squared interband matrix element $M$ in the vicinity of the $U$ and $U'$ points is :

$$|P_{v\to c}|^2 = \frac{9}{8}\gamma_0^2 b^2 \frac{m^2}{\hbar^2}\,. \quad (23)$$

In the range of validity of the linear dispersion relations (8) for initial and final electronic states (which corresponds to the photon energy region $\hbar\omega \lesssim \gamma_0$), the imaginary part of $\varepsilon_{\text{inter}}$ is :

$$\text{Im}\ \varepsilon_{\text{inter}} = \frac{\pi e^2}{d\hbar\omega}\,. \quad (24)$$

This particular frequency dependence of Im $\varepsilon_{\text{inter}}$ implies a nearly constant value of Re $\varepsilon_{\text{inter}}$ in this energy region.

If the formula (24) were valid for all photon energies, the real part Re $\varepsilon_{\text{inter}}$ would be equal to zero independently of the frequency $\omega$. In reality, the interband transitions at the saddle point ($W$ point of the B.Z.) at photon energies $\hbar\omega \approx 2\gamma_0$ give an important contribution to Re $\varepsilon_{\text{inter}}$. This contribution should be nearly constant in the range of frequencies ($\hbar\omega < \gamma_0$) considered in this paper.

The frequency dependence of the real and imaginary parts established experimentally by Taft and Philipp [12] shows that the real part of the dielectric function is indeed nearly constant for photon energies between 0.8 and 3.5 eV : $\varepsilon_0 = 4.4$.

Instead of calculating Re $\varepsilon_{\text{inter}}$ which would require a knowledge of the wavefunctions and energies over the entire Brillouin zone, we identify Re $\varepsilon_{\text{inter}}$ with $\varepsilon_0$ and we approximate the complex dielectric function of graphite by

$$\varepsilon_\perp^0(\omega) = \varepsilon_0 + \frac{i\pi e^2}{d\hbar\omega}\,. \quad (25)$$

The figure 7 presents the comparison between the frequency dependence of the reflectivity calculated from (25) and the experimental data [5, 12]. The excellent agreement over a broad frequency region constitues a strong support for the model which we propose for lowest stages of GAC.

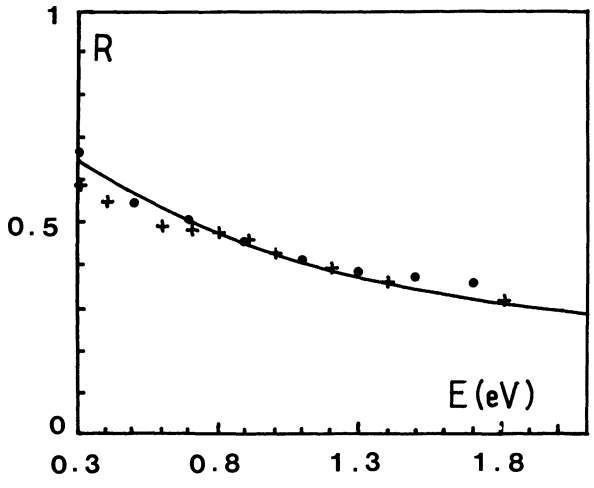


Fig. 7. — Reflectivity spectrum of pure graphite. Solid line : calculated line (25) ; points from Ref. [5], crosses from Ref. [12].

3.2 FIRST STAGE. — The interband contribution is still given by (22) with $n = 1$, and with the square of the matrix element $|P_{v\to c}|^2$ given by (23). The threshold of the interband transitions is located at $\hbar\omega = 2E_F$.

The lack of real interband transitions at $\hbar\omega < 2E_F$ introduces an additional frequency dependent term in Re $\varepsilon_{inter}$ which (at $T = 0$ K and without damping) has a logarithmic singularity at $\hbar\omega = 2E_F$. For $kT \ll E_F$, the intraband contribution to the dielectric function can be expressed as :

$$\varepsilon_{inter}(\omega) - 1 = \frac{d}{I_c}[\varepsilon_\perp^0(\omega) - 1] - \Delta\varepsilon$$

where $\Delta\varepsilon$ is the contribution from the transitions $v \to c$ which are excluded due to the depopulation of the valence level :

$$\Delta\varepsilon = + \lim_{s\to 0^+} \frac{e^2}{I_c \hbar\omega} \times$$

$$\times \int_0^\infty \left(\frac{1}{y - \hbar\omega - is} - \frac{1}{y + \hbar\omega + is}\right) \frac{dy}{1 + e^{(y-2E_F)/2k_BT}}.$$

At $T = 0$ K, we have

$$\Delta\varepsilon = -\frac{e^2}{I_c \hbar\omega} \times$$

$$\times \lim_{s\to 0^+} [\ln(\hbar\omega + is + 2E_F) - \ln(\hbar\omega + is - 2E_F)]. \quad (26)$$

For $T \neq 0$ K, only Im $\Delta\varepsilon$ can be evaluated exactly :

$$\text{Im}\,\Delta\varepsilon = + \frac{\pi e^2}{I_c \hbar\omega} \frac{1}{1 + e^{(\hbar\omega - 2E_F)/2k_BT}} \quad (\omega > 0). \quad (27)$$

The analytical properties of $\Delta\varepsilon(\omega)$ in the complex $\omega$ plane are the same as they should be for the most general dielectric function $\varepsilon(\omega) - 1$ thus Re $\Delta\varepsilon$ for a real $\omega$ is entirely determined by Im $\Delta\varepsilon$ along the entire real axis.

For any $T$, the function $\Delta\varepsilon$ can therefore be well approximated by the function :

$$-\frac{e^2}{I_c \hbar\omega}[\ln(\hbar\omega + i2k_BT + 2E_F) - \ln(\hbar\omega + i2k_BT - 2E_F)]$$

which has desired analytical properties, coincides with (26) as $T \to 0$ and whose imaginary part for any $T$ approximates quite well the exact formula (27) along the entire real axis.

The real part of the total dielectric function, including the intraband contribution is :

$$\text{Re}\,\varepsilon_\perp(\omega) = 1 + \frac{d}{I_c}(\varepsilon_0 - 1) + \frac{e^2}{2I_c\hbar\omega} \times$$

$$\times \ln\left[\frac{(2E_F + \hbar\omega)^2 + 4k_B^2T^2}{(2E_F - \hbar\omega)^2 + 4k_B^2T^2}\right] - \frac{4e^2E_F}{I_c\hbar^2(\omega^2 + 1/\tau^2)}$$

$\varepsilon_0$ is the real part of the dielectric function of pure graphite within the 2D model. $\hbar/\tau$ is a damping constant introduced phenomenologically in the intraband term (20) to account for carrier scattering. The imaginary part of $\varepsilon_\perp(\omega)$ is :

$$\text{Im}\,\varepsilon_\perp(\omega) = \frac{\pi e^2}{I_c\hbar\omega}\left[1 + \frac{1}{\pi}\text{arc ctg}\left(\frac{\hbar\omega + 2E_F}{2k_BT}\right) - \right.$$

$$\left. - \frac{1}{\pi}\text{arc ctg}\frac{\hbar\omega - 2E_F}{2k_BT}\right] + \frac{4e^2E_F}{I_c\omega\tau\hbar^2(\omega^2 + 1/\tau^2)}$$

here $0 \leqslant \text{arc ctg} \leqslant \pi$. When $T \to 0$, the function in square brackets tends to the simple step function $\theta(\hbar\omega - 2E_F)$.

3.3 SECOND STAGE. — The interlayer interaction removes partially the band degeneracy at the $U$ point, as a result several types of intraband transitions are possible : the intervalence transitions $v_1 \to v_2$ at $\hbar\omega = \gamma_1$ and the valence to conduction band transitions $v_2 \to c_2$, $v_1 \to c_2$ with the threshold at $\hbar\omega = 2E_F$, $v_2 \to c_1$ and $v_1 \to c_2$ with the thresholds at $\hbar\omega = 2E_F - \gamma_1$, and $2E_F + \gamma_1$ respectively. Close to the $U$ and $U'$ points, the squared matrix elements calculated from the wavefunctions (16) are :

$$|P_{v_2\to v_1}|^2 = |P_{v_2\to c_1}|^2 = |P_{v_1\to c_2}|^2 =$$

$$= \frac{\gamma_1^2}{\gamma_1^2 + 9\gamma_0^2b^2k^2}|P_{v\to c}|^2, \quad (28)$$

$$|P_{v_2\to c_2}|^2 = |P_{v_1\to c_1}|^2 = \frac{9\gamma_0^2b^2k^2}{\gamma_1^2 + 9\gamma_0^2b^2k^2}|P_{v\to c}|^2 \quad (29)$$

where $|P_{v\to c}|^2$ is given by (23). For $E_F > \gamma_1$, one can expect from these formulae the threshold for $v_1 \to c_1$ and $v_2 \to c_2$ transitions at $\hbar\omega = 2E_F$ to be much more pronounced than the remaining two. For $kT \ll E_F$ and $\gamma_1 \ll 2E_F$, the real and imaginary parts of $\varepsilon_\perp(\omega)$ for the second stage, including the intraband contribution are

$$\operatorname{Re}\varepsilon_{\perp}(\omega) = 1 + \frac{2\,d(\varepsilon_0 - 1)}{I_c + d} + \frac{e^2}{(I_c + d)\,\hbar\omega}\left(1 - \frac{\gamma_1^2}{\hbar^2\,\omega^2}\right) F_1(2\,E_F) + \\ + \frac{e^2\,\gamma_1^2}{2(I_c + d)\,\hbar^3\,\omega^3}\,[F_1(2\,E_F - \gamma_1) + F_1(2\,E_F + \gamma_1)] \\ + \frac{e^2\,\gamma_1^2}{(I_c + d)\,\hbar\omega E_F}\left(\frac{1}{\gamma_1 - \hbar\omega} - \frac{1}{\gamma_1 + \hbar\omega}\right) - \frac{8\,e^2\,E_F}{(I_c + d)\,\hbar^2(\omega^2 + 1/\tau^2)}\left(1 - \frac{\gamma_1^2}{4\,E_F^2}\right) \quad (30)$$

$$\operatorname{Im}\varepsilon_{\perp}(\omega) = \frac{2\,\pi e^2}{(I_c + d)\,\hbar\omega}\left(1 - \frac{\gamma_1^2}{\hbar^2\,\omega^2}\right) F_2(2\,E_F) + \frac{\gamma_1^2\,e^2\,\pi}{(I_c + d)\,\hbar^3\,\omega^3}\,[F_2(2\,E_F - \gamma_1) + F_2(2\,E_F + \gamma_1)] + \\ + \frac{e^2\,\gamma_1^2\,\pi}{(I_c + d)\,\hbar\omega E_F}\,\delta(\hbar\omega - \gamma_1) + \frac{8\,e^2\,E_F}{(I_c + d)\,\omega\tau\hbar^2(\omega^2 + 1/\tau^2)}\left(1 - \frac{\gamma_1^2}{4\,E_F^2}\right) \quad (31)$$

where we have introduced the following abbreviations :

$$F_1(x) = \ln\left|\frac{(\hbar\omega + x)^2 + 4\,k_B^2\,T^2}{(\hbar\omega - x)^2 + 4\,k_B^2\,T^2}\right|$$

$$F_2(x) = 1 + \frac{1}{\pi}\operatorname{arc\,ctg}\left(\frac{\hbar\omega + x}{2\,k_B\,T}\right) - \\ - \frac{1}{\pi}\operatorname{arc\,ctg}\left(\frac{\hbar\omega - x}{2\,k_B\,T}\right).$$

For $T \to 0$, the function $F_2(x)$ tends to the standard step function $\theta(\hbar\omega - x)$.

In deriving (30) and (31) we have neglected the terms in higher than second orders of $\gamma_1/2\,E_F$.

Both real and imaginary parts of $\varepsilon_{\perp}$ are divergent at $\hbar\omega = \gamma_1$. These divergences, resulting from the use of simplified dispersion relations (15) for the valence bands, will disappear if one uses more complete dispersion relations (14) and/or if one takes into account carrier scattering.

It is interesting to observe that the dielectric function in all three cases of pure graphite, 1st and 2nd stage GAC does not depend on the value of the intralayer resonance integral $\gamma_0$. This integral appears only in the formulae relating the Fermi energy $E_F$ to the charge transfer coefficient $f$.

4. **Experimental details.** — The electron-acceptor graphite intercalation compounds are usually prepared under a controlled atmosphere in pyrex glass tubes using the two temperature furnace technique (Fig. 8) [13]. The following parameters are thus held fixed during the reaction : the temperature $T_R$ of the reagent (in excess) and the temperature $T_C$ of the compounds.

$T_R$ determines the vapour pressure $P_0$ of the reagent in its free state and $T_c$ the vapour pressure $P$ of the intercalated reagent. By carefully choosing $T_C$ and $T_R$, the ratio $P/P_0$ can be varied and in certain cases defined compounds can be prepared (Fig. 9).

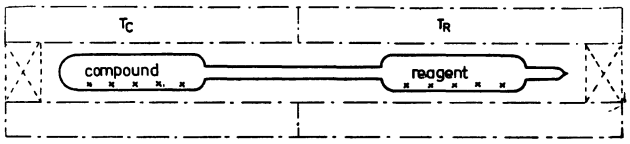


Fig. 8. — Reaction tube : $T_c$ temperature of compound ; $T_R$ temperature of reagent to be intercalated.

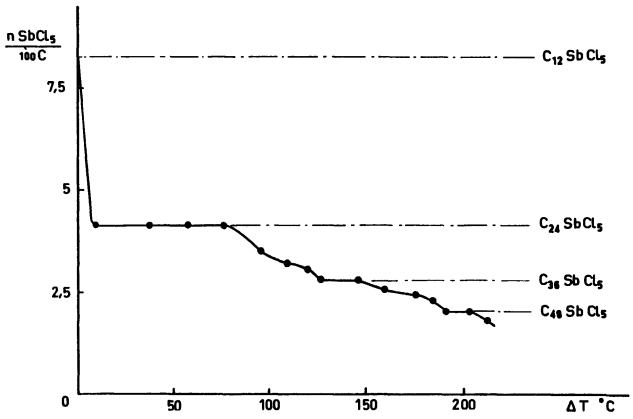


Fig. 9. — Desorption isotherm of a graphite-$SbCl_5$ compound : $T_C = 217$ °C, $T = T_C - T_R$.

Each compound is characterized by its composition, its identity period (distance separating two intercalant layers), its interplanar distance (the distance separating the two carbon planes adjacent to the intercalant) and its stage (number of carbon layers separating two layers of intercalant).

When thermodynamic equilibrium has been obtained, often after several days, the reaction tube is separated into two parts by sealing off the intermediate section. The intercalation compound is thus prepared, *in situ*, in a sample holder adapted to the measuring instruments and may be perfectly maintained in the presence of the intercalant in its vapour state.

Each sample is identified by sensitive x-ray crystallographic methods perfected in the laboratory [14] : the $00\ell$ reflection diagrams are reproducible and allow determining with certainty the stage and purity of the compounds prepared to be determined certainly (table I) (Fig. 10).

Table I. — *Compounds studied.*

| Formula of the compound | Ref. | Stage | Identity period (Å) | $T_R$ (°C) | $T_c$ (°C) |
|---|---|---|---|---|---|
| $C_{24}SbCl_5$ | [15] | 2 | 12.72 | 210 | 240 |
| $C_8Br$ | [16] | 2 | 10.4 | 20 | 25 |
| $C_8I_{0.45}Cl_{0.55}$ | [17] | 2 | 10.69 | 20 | 38 |

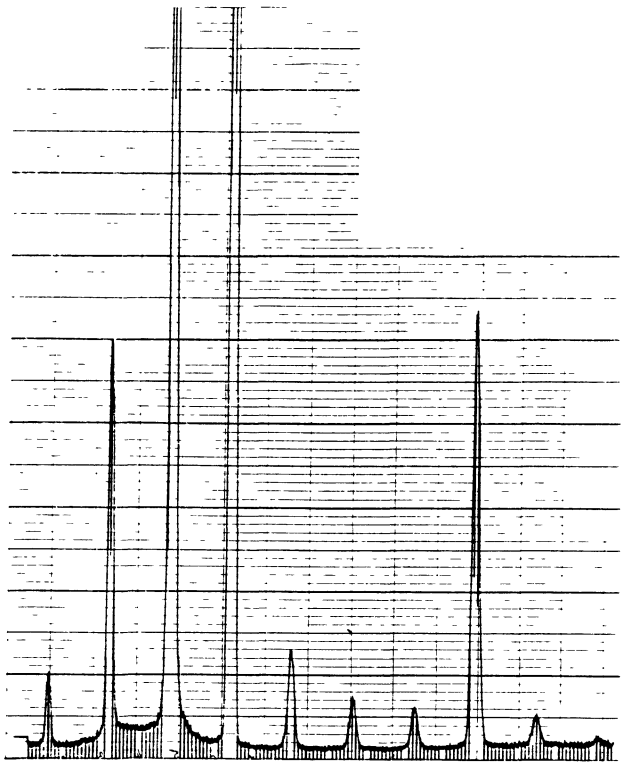

Fig. 10. — $00\ell$ reflection diagram for $C_{24}SbCl_5$ (second stage).

Reflectivity measurements were performed at normal incidence with unpolarized $\varepsilon \perp c$ radiation, in the spectral region 0.1-3 eV, using grating spectrometers and cooled photodetectors (PbS, InSb, Golay cell). To avoid any desorption process, measurements were made on samples in the original pyrex reaction tube (below 0.5 eV, a $F_2Ca$ window was used), which were sealed after intercalation.

5. **Experimental results and discussion.** — Our experimental reflectivity curves for the 2nd stage of several GAC are shown in figures 11, 12, 13. In all materials, a metallic reflectance is observed in the low frequency region followed by the plasma edge with well pronounced minima in the 1.1 eV energy region for second stage compounds. At higher energies, $R(E)$ is nearly flat and in some cases exhibits a slow decrease in the high frequency region.

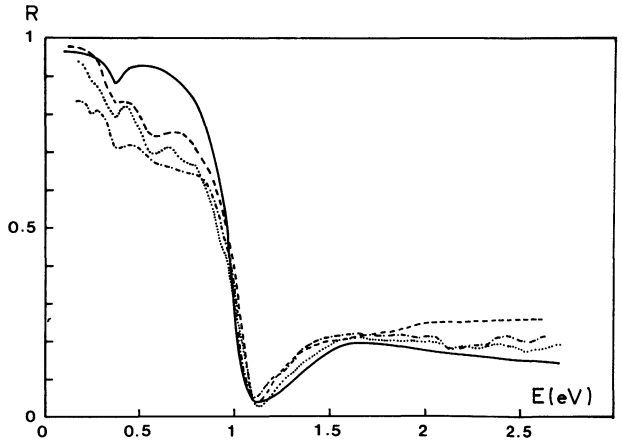


Fig. 11. — Reflectance spectra for three different samples of $C_{24}SbCl_5$. Solid line : theory ; Broken lines : experiments.

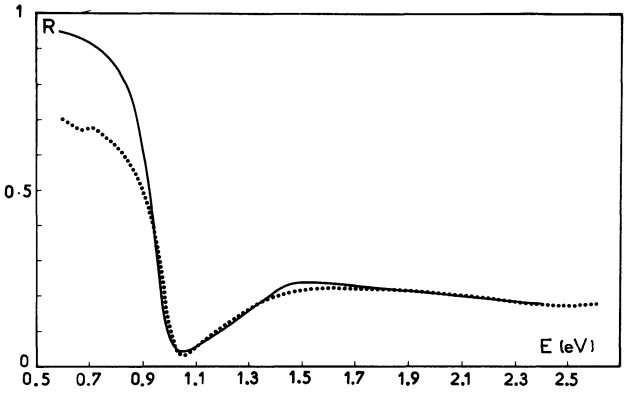


Fig. 12. — Reflectance spectrum of $C_{16}Br_2$. Solid line : theory ; Broken line : experiment.

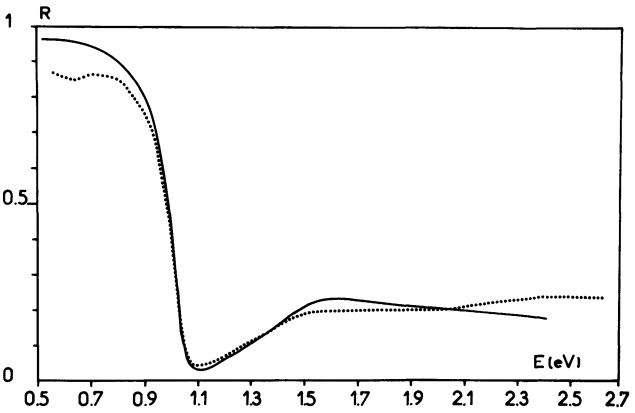


Fig. 13. — Reflectance spectrum of $C_{16}ICl$. Solid line : theory ; Broken lines : experiment.

We show in figure 11 the reproductibility of the spectra for three different samples of $SbCl_5$-graphite : the curves coincide in the region of the plasma edge,

in particular minima occur at the same energy. One can observe however slight differences in the low and high frequency regions ($\hbar\omega < 0.8$ eV or $> 2$ eV).

In the low energy region, a reflectance minimum is systematically observed near $\hbar\omega = 0.37$ eV, for all second stage samples investigated in this region. This minimum is a characteristic feature of stage 2. and does not show up in higher stage compounds nor in pure graphite. We observe also another structure near 0.56 eV, which is not evident in all spectra. The observation of this latter structure was also reported by Shieh [18] for higher stages of $HNO_3$-graphite and other compounds.

For a quantitative analysis of the reflectance data, we use the theory developed in section 3, with $\gamma_1 = 0.377$ eV [19].

The real and imaginary parts of $\varepsilon(\omega)$ depend on the Fermi energy $E_F$ and damping factor $1/\tau$.

In the first stage, at energies $\hbar\omega < 2\,E_F$ the dielectric function is dominated by the intraband contribution. At $\hbar\omega > 2\,E_F$, the reflectance spectrum is mostly determined by Im $\varepsilon(\omega)$ which becomes important due to strong interband transitions similarly to those of pure graphite. In particular, the frequency dependence of Im $\varepsilon_\perp(\omega)$ implies the slow decrease of $R(E)$ in the high frequency region. The position of the reflectance minimum drastically depends on $E_F$ which enters in both intra and interband contributions.

Qualitatively, the same behavior is expected for second stage compounds, as the strongest interband contribution originates from $v_1 \to v_1$ and $v_2 \to c_2$ transitions with a threshold at $\hbar\omega = 2\,E_F$. The thresholds at $\hbar\omega = 2\,E_F \pm \gamma_1$ are less important. An additional effect is observed in stage 2, due to intervalence transitions : a peak should appear at $\hbar\omega = \gamma_1$ which is in excellent agreement with the observation of the reflectance minimum at 0.37 eV. This effect constitutes a strong support of the validity of our model. By fitting $E_F$ and $\tau$, one reproduces quite well the frequency dependence of the reflectivity throughout the entire investigated spectral region. The structure at 0.56 eV remains however unexplained. The comparison between theory and experiments is shown in figures 11-13 for stage 2 of different GAC. We also include in the present analysis the experimental results published by Hanlon *et al.* [3] on stage 1 and 2 of $AsF_5$-graphite (Fig. 14). The latter experiment is however restricted to energies lower than $2\,E_F$. In calculating $R(\omega)$, we introduce in (28, 31) an effective temperature $T_{eff}$ larger than the experimental temperature to phenomenologically account for the effect of scattering associated with interband transition. In plotting figures 11-14 the Dirac singularity at $\hbar\omega = \gamma_1$ is removed using a Lorentzian lineshape with the experimental width appropriate for $SbCl_5$. In figures 11-14, the following values of the parameters have been used :

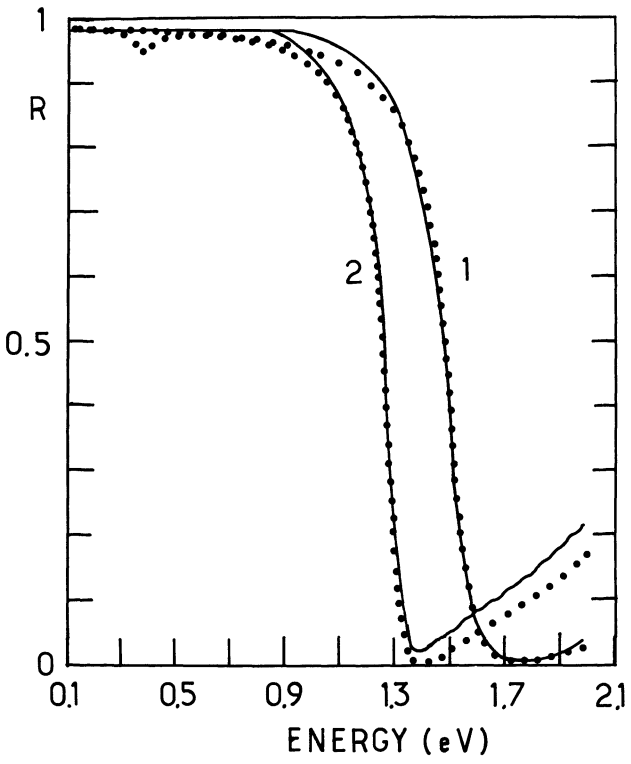


Fig. 14. — Reflectance spectra of $C_8AsF_5$ (I) and $C_{16}AsF_5$ (II). Solid lines : experiments from Ref. [3] ; dotted lines : theory.

Table II.

| | $2\,E_F$ (eV) | $\tau$ | $T_{eff}$ | $f$ |
|---|---|---|---|---|
| | — | — | — | — |
| $C_{24}SbCl_5$ | 1.5 | $1.10^{-14}$ | 600 | 0.25-0.44 |
| $C_{16}Br_2$ | 1.4 | $3.10^{-14}$ | 450 | 0.15-0.25 |
| $C_{16}ICl$ | 1.5 | $3.10^{-14}$ | 450 | 0.17-0.29 |
| $C_8AsF_5$ | 2.6 | $7.10^{-15}$ | 450 | 0.26-0.44 |
| $C_{16}AsF_5$ | 2 | $3.10^{-14}$ | 450 | 0.3 -0.51 |

The fractional charge transfer coefficient $f$ reported in the last column of table II is determined from the hole Fermi energy $E_F$ using the relations (11) and (17). The lower and upper limits of $f$ correspond to the values of $\gamma_0 = 3.12$ eV [19] and 2.4 eV respectively. The higher value of $\gamma_0$ is established by analysing the properties of carriers close to the Fermi level in pure graphite in the framework of the complete Slonczewski-Weiss model including several additional parameters neglected in our simplified model. In the framework of the simplified model, the lower value $\gamma_0$, which was chosen to reproduce the band structure along the W-U line of the BZ (see Fig. 3) seems to be more appropriate. The values of $f$ for $AsF_5$ are similar to those established by magnetic resonance studies by Weinberger *et al.* [20] but the change of $f$ when passing from the first to the second stage is less pronounced here.

**Acknowledgment.** — We thank Dr. A. Moore for supplying us with HOPG.

## References


[1] FISCHER, J. E., THOMPSON, T. E., FOLEY, G. M. T., GUÉRARD, D., HOKE, M. and LEDERMAN, F. L., *Phys. Rev. Lett.* **37** (1976) 769.

[2] THOMPSON, T. E., FALARDEAU, E. R. and HANLON, L. R., *Carbon* **15** (1977) 39.

[3] HANLON, L. R., FALARDEAU, E. R., GUÉRARD, D., FISCHER, J. E., *Materials Science and Engineering* **31** (1977) 161.

[4] BATALLAN, F., BOK, J., ROSENMAN, I. and MELIN, J., *Phys. Rev. Lett.* **41** (1978) 330.
ROSENMAN, I., BATALLAN, F. and FURDIN, G., *Phys. Rev.* (in press).

[5] FISCHER, J. E., *Physics and Chemistry of Materials with Layered Structures*, Vol. 5, F. Levy, editor (D. Reidel, Dordrecht, Holland).

[6] WALLACE, P. R., *Phys. Rev.* **71** (1947) 622.

[7] PAINTER, G. S. and ELLIS, D. E., *Phys. Rev.* **B 1** (1970) 4747.

[8] TSUKADA, M., NAKAO, K., UEMURA, Y. and NAGAI, S., *J. Phys. Soc. Japan* **32** (1972) 54.

[9] JOHNSON, L. G. and DRESSELHAUS, G., *Phys. Rev.* **B 7** (1973) 2275.

[10] BASSANI, F., PASTORI-PARRAVICINI, G., *Nuovo Cimento* **50B** (1967) 95.

[11] SLONCZEWSKI, J. C. and WEISS, P. R., *Phys. Rev.* **99** (1955) A 636.

[12] TAFT, E. A. and PHILIPP, H. R., *Phys. Rev.* **138** (1965) A 197.

[13] HÉROLD, A., *Bull. Soc. Chim. Fr.* **187** (1955) 299.

[14] GUÉRARD, D., LE COURAIN, N. and AUBRY, A., *Bull. Soc. Franc. Min. et Cristall.* **98** (1975) 43.

[15] MELIN, J. and HÉROLD, A., *Carbon* **13** (1975) 357.

[16] BACH, B., BAGOUIN, N., BLOC, F. et HÉROLD, A., *C.R. Hebd. Séan. Acad. Sci.* **257** (1963) 681.

[17] BACH, B. et HÉROLD, A., *Bull. Soc. Chim. Fr.* **5** (1968) 1978.

[18] SHIEH, Ç. C., SCHMIDT, R. L. and FISCHER, J. E., Proceedings of the 14th Biennial Conference of Carbon, University Park, Pennsylvania, June 1979. To be published in Carbon.

[19] DRESSELHAUS, M. S., DRESSELHAUS, G., FISCHER, J. E., *Phys. Rev.* **B 15** (1977) 3180.

[20] WEINBERGER, B. R., KAUFER, J., HEEGER, A. J., FISCHER, J. E., MORAU, M. and HOLZWARTH, N. A. W., *Phys. Rev. Lett.* **41** (1978) 1417.